Electronic Supplementary Information

Use of titanocalix[4]arenes in the ring opening polymerization of cyclic esters

Ziyue Sun,[a] Yanxia Zhao,[a*] Orlando Santoro,[b] Mark R. J. Elsegood,[c] Elizabeth V. Bedwell,[c] Khadisha Zahra,[d] Alex Walton,[d] and Carl Redshaw[a,b*]

[a] *College of Chemistry and Material Science, Northwest University, 710069 Xi'an, China*

[b] *Department of Chemistry and Biochemistry, The University of Hull, Cottingham Rd, Hull, HU6 7RX, U.K.*

[c] *Chemistry Department, Loughborough University, Loughborough, Leicestershire, LE11 3TU, U.K.*

[d] *Department of Chemistry, University of Manchester, Oxford Road, Manchester, M13 9PL, UK.*

Contents

Figure S7. ^{1}H NMR spectrum ($CDCl_3$, 400 MHz, 298 K) of the PCL synthesized with **5** in the absence of BnOH under N_2.

Figure S8. MALDI-TOF spectrum of the PCL synthesizes in with **5**/BnOH under N_2.

Figure S9. MADI-TOF spectrum of the PCL synthesized with **5**/BnOH in air.

Figure S10. MALDI-TOF spectrum of the PCL synthesized with **5**/BnOH in the absence of BnOH under N_2.

Figure S11. ^{1}H NMR spectrum ($CDCl_3$, 400 MHz, 298 K) of the PVL synthesized with **5**/BnOH under N_2

Figure S12. ^{1}H NMR spectrum ($CDCl_3$, 400 MHz, 298 K) of the PVL synthesized with **5**/BnOH in air.

Figure S13. 2D J-resolved ^{1}H NMR spectrum ($CDCl_3$, 400 MHz, 298 K) of the PLA synthesized with **1**.

Figure S14. 2D J-resolved ^{1}H NMR spectrum ($CDCl_3$, 400 MHz, 298 K) of the PLA synthesized with **2**.

Figure S15. 2D J-resolved ^{1}H NMR spectrum ($CDCl_3$, 400 MHz, 298 K) of the PLA synthesized with **3**.

Figure S16. 2D J-resolved ^{1}H NMR spectrum ($CDCl_3$, 400 MHz, 298 K) of the PLA synthesized with **4**.

Figure S17. 2D J-resolved ^{1}H NMR spectrum ($CDCl_3$, 400 MHz, 298 K) of the PLA synthesized with **5**.

Figure S18. ^{1}H NMR spectrum ($CDCl_3$, 400 MHz, 298 K) of the poly-PDL.

Figure S19. ^{1}H NMR spectrum ($CDCl_3$, 400 MHz, 298 K) of the CL-VL Copolymer (1:1 ratio CL/VL).

Figure S20. ^{13}C NMR spectrum (CDCl3, 400 MHz, 298 K) of the CL-VL Copolymer (65-63 ppm).

Equation S1 Determination of number-average sequence length for CL.

Equation S2. Determination of number-average sequence length for VL.

Equation S3. Determination of the Randomness Character (*R*).

Figure S21. DSC curve of the CL/VL copolymer.

Figure S22. ^{1}H NMR spectrum ($CDCl_3$, 400 MHz, 298 K) of the CL/LA (500:50) co-polymer.

Figure S23. ^{1}H NMR spectrum ($CDCl_3$, 400 MHz, 298 K) of CL/LA co-polymer 75% PLA: 35% PCL – unreacted ε-CL).

Figure S24. Carbonyl range of ^{13}C NMR spectrum ($CDCl_3$, 25 ºC) of CL/LA co-polymer 75% PLA: 35%.

Crystallographic experimental details.

The following section gives details of disorder and solvent of crystallization modelling for the individual crystal structures.

For **2·2MeCN**: ^{t}Bu group at C(18) modelled as having the methyl groups disordered over two sets of positions with major occupancy 54.6(4)%.

For **4·6MeCN**: ^{t}Bu group at C(40) modelled with two fold disorder of the methyl groups with major component occupancy 59.1(11)%. The two terminal atoms, C(53), C(54) on one decyl chain were also modelled as two fold disorder with major component occupancy 69(2)%. MeCN containing N(4) was modelled at 50% occupancy. MeCN group at N(1) was modelled with two fold disorder of atoms N(1) and C(56) with major component occupancy 56.1(8)%. In the asymmetric unit 3.5 MeCNs were modelled as point atoms, while the other 2.5 were modelled as diffuse areas of electron density via the Platon squeeze procedure.

For **6·7MeCN**: ^{t}Bu group at C(18) was modelled with Me groups disordered over two sets of positions with major component 56.3(15)%. The ^{t}Bu group at C(7) also showed signs of disorder though this was not modelled; the geometry is not quite ideal in the latter case. ^{n}Pr groups exit either at O(5) and O(1) {64.8(6)% occupancy} as shown in the fig, or at O(3) and O(7) {35.2(6)% occupancy}. MeCN at N(5) was modelled a disordered over two sets of positions with major component occupancy of 66.7(10)%. MeCN at N(2) was modelled at 50% occupancy due to the proximity of peaks nearby (see Squeeze later). MeCN at N(3) had the occupancy refined, then fixed at 0.8 due to the proximity of several residual electron density peaks showing this MeCN might exist in many different orientations in this cavity close to the OH group. Platon Squeeze recovered 126 electrons in 2 voids. MeCN has 22 electrons, so an extra 5.4 MeCNs were added to the formula which tied in with the partial occupancy of the MeCN at N(3) giving 7 MeCNs of crystallisation overall.

For **7·7.5MeCN**: ^{t}Bu groups at C(67) and C(78) were modelled with Me groups split over two sets of positions with major occupancies 68.3(8) and 70.1(12)% respectively. The MeCN at N(2) was modelled as fully disordered over two sets of positions a short distance apart with a calix cavity with major occupancy 66.5(5)%. The MeCN at N(6) was modelled at half weight as it was very diffuse or partially occupied.

For **8·11MeCN**: ^{t}Bu groups at C(56) and C(89) modelled as disordered with the Me groups split over two sets of positions with major occupancies of 56.6(8) and 58.5(13)% respectively. Non-coordinated MeCNs of crystallisation at N(7), N(8), & N(9) were modelled with 50% occupancy due to partial occupancy or underlying disorder.

For **9·9MeCN**: Two of the MeCNs modelled as a diffuse area of electron density by the Platon Squeeze procedure due to severe disorder. These were located in the calix[4]arene cavity adjacent to Ti(1). One ^{t}Bu group at C(18) modelled as having the methyl groups two-fold disordered with major occupancy 69.0(7)%.

For **10·8.5MeCN**: The ^{t}Bu groups at C(83) and C(94) were modelled with two sets of positions for the Me groups with major occupancies of 53(2) and 70.1(13)% respectively. The ^{t}Bu group at C(4) was modelled as fully disordered over two sets of positions with major occupancy 75.4(11)%. 8.5 MeCNs of crystallisation, one of which is H-bonded to the bridging OH group. MeCNs at N(8), N(9), and N(10) were modelled at half occupancy as they were rather diffuse.

For **11·2.85MeCN·0.43H_2O**: The bridging chloride and hydroxyl groups are two-fold disordered with the major components occupied 56.8(3)% of the time. The major component OH^- forms an H-bond with an NCMe solvent molecule of crystallisation, but the minor component on the opposite side of the molecule forms an H-bond with a single atom entity, modelled as a water molecule for which the H atoms were not refined. For the major occupancy Cl^-, there is an NCMe solvent of crystallisation nearby {including N(4)}, disordered over a centre of symmetry. The ^{t}Bu groups at C(18), C(56), and C(78) were modelled with the methyl groups split over two sets of positions with major occupancies 70.6(10), 66.7(7), 53.3(8)% respectively.

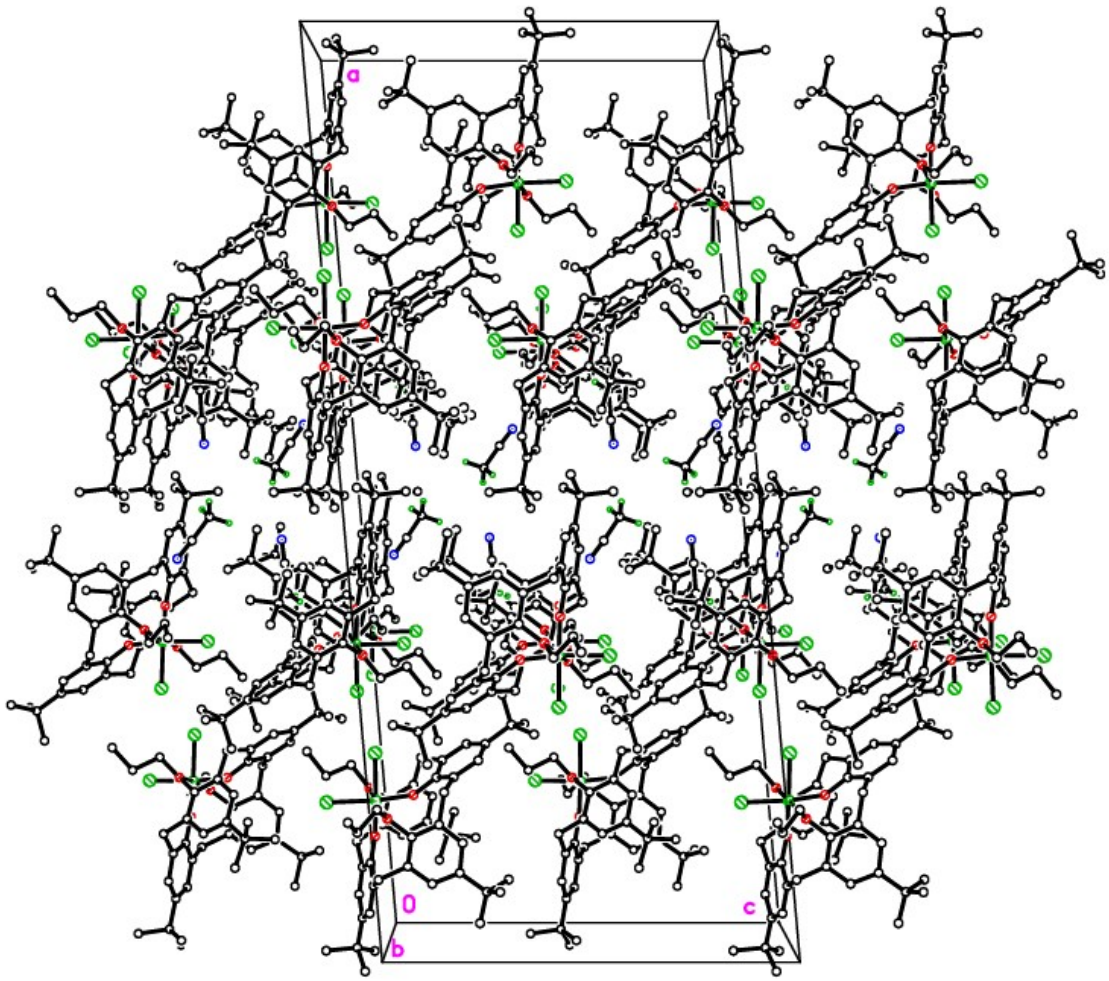

Figure S1. The molecules of $[TiCl_2(L(O)_2(O\textit{n}\text{-}Pr)_2]\cdot 2MeCN$ (**2**·2MeCN) pack in anti-parallel layers.

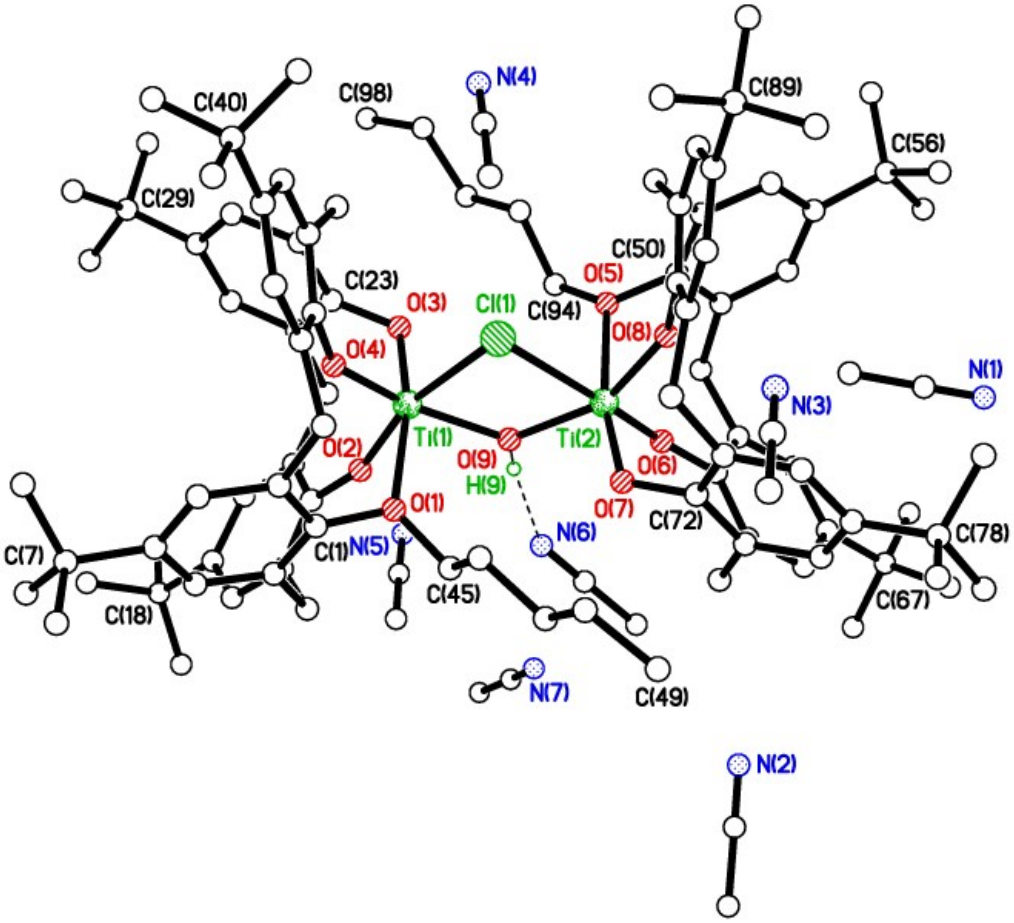

Figure S2. Molecular structure of {[TiL(O)$_3$(O*n*-pentyl)]$_2$(μ-Cl)(μ-OH)}·9MeCN **9**·9MeCN. Selected bond lengths (Å) and angles (°): Ti(1)–O(1) 2.3646(17), Ti(1)–O(2) 1.7949(17), Ti(1)–O(3) 1.8415(17), Ti(1)–O(4) 1.8197(16), Ti(1)–O(9) 1.9882(17), Ti(1)–Cl(1) 2.5155(7); O(1)–Ti(1)–O(3) 169.39(7), O(2)–Ti(1)–O(4) 104.87(8), Cl(1)–Ti(1)–O(9) 73.95(6), Ti(1)–O(1)–C(1) 112.71(13), Ti(1)–O(2)–C(12) 162.28(16), Ti(1)–O(3)–C(23) 120.86(14), Ti(1)–O(4)–C(34) 147.53(15).

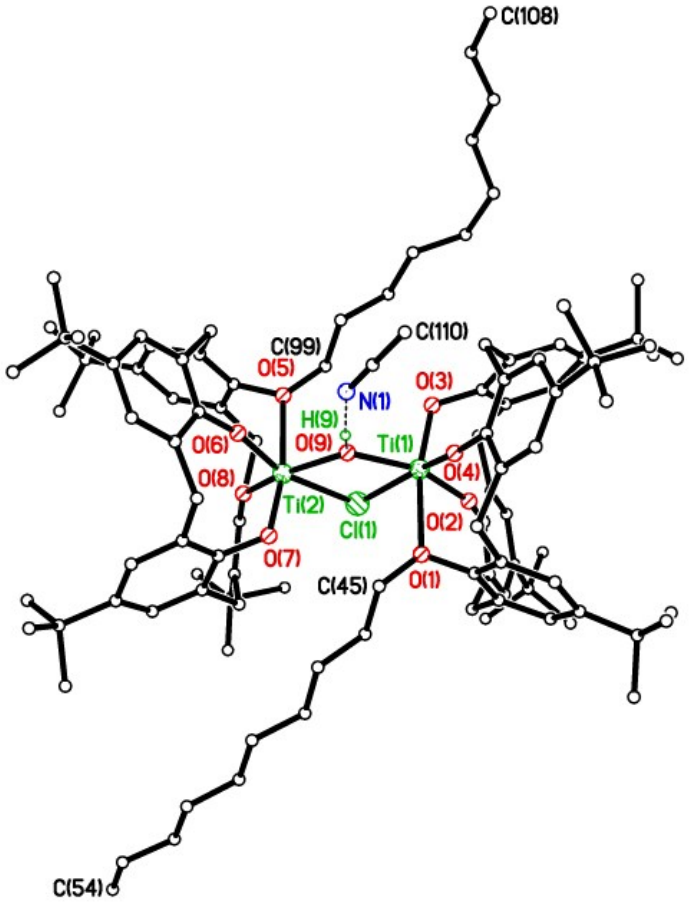

Figure S3. Alternative views of {[TiL(O)$_3$(O*n*-decyl)]$_2$(μ-Cl)(μ-OH)}·8.5MeCN (**10**·8.5MeCN).

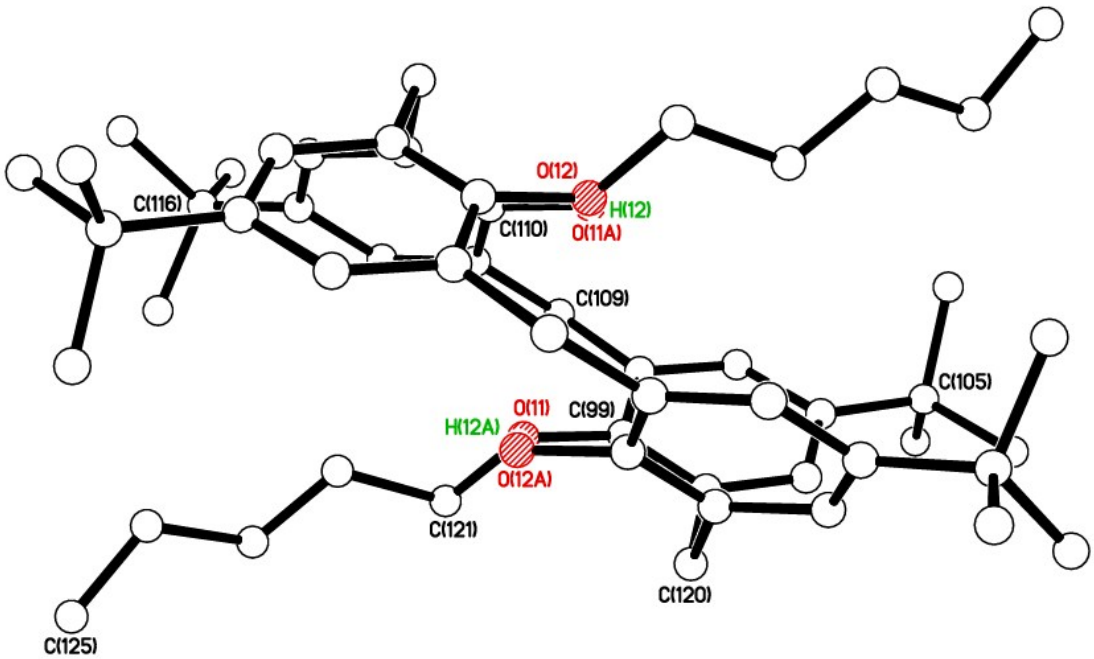

Figure S4. End on view of [L(OH)$_2$(OR)$_2$] in (**11**·2.85(MeCN)·0.43(H_2O)).

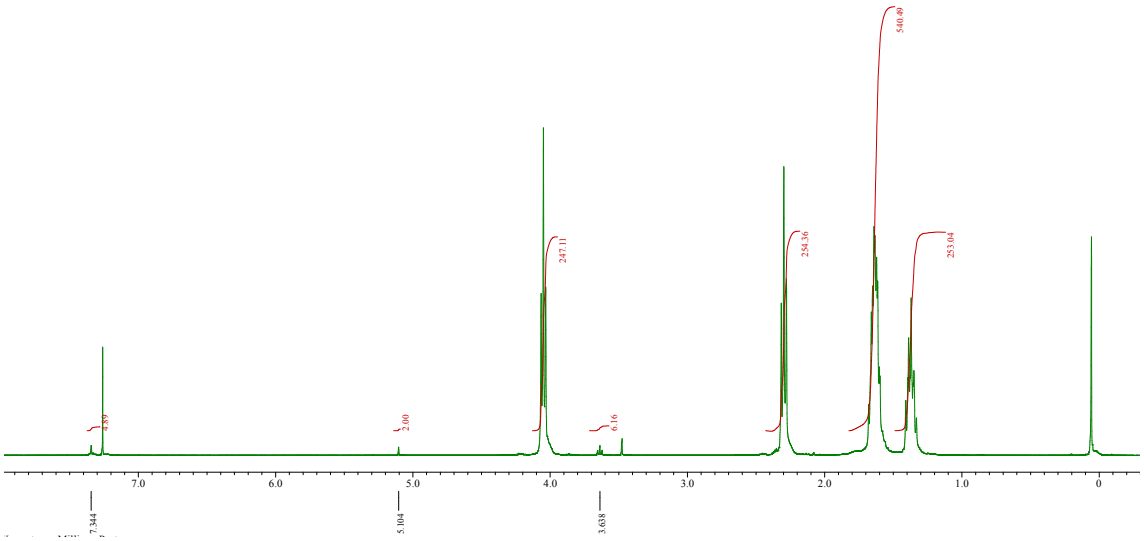

Figure S5: ^{1}H NMR spectrum ($CDCl_3$, 400 MHz, 298 K) of the PCL synthesised with **5**/BnOH under N_2.

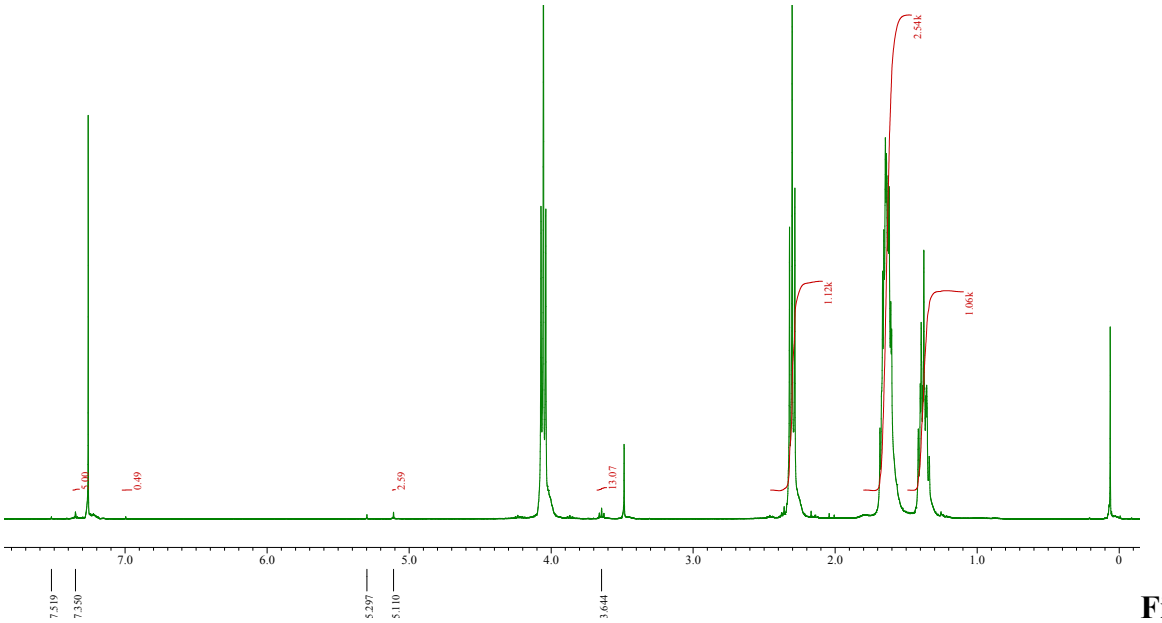

Figure S6: ^{1}H NMR spectrum ($CDCl_3$, 400 MHz, 298 K) of the PCL synthesised with **5**/BnOH in air.

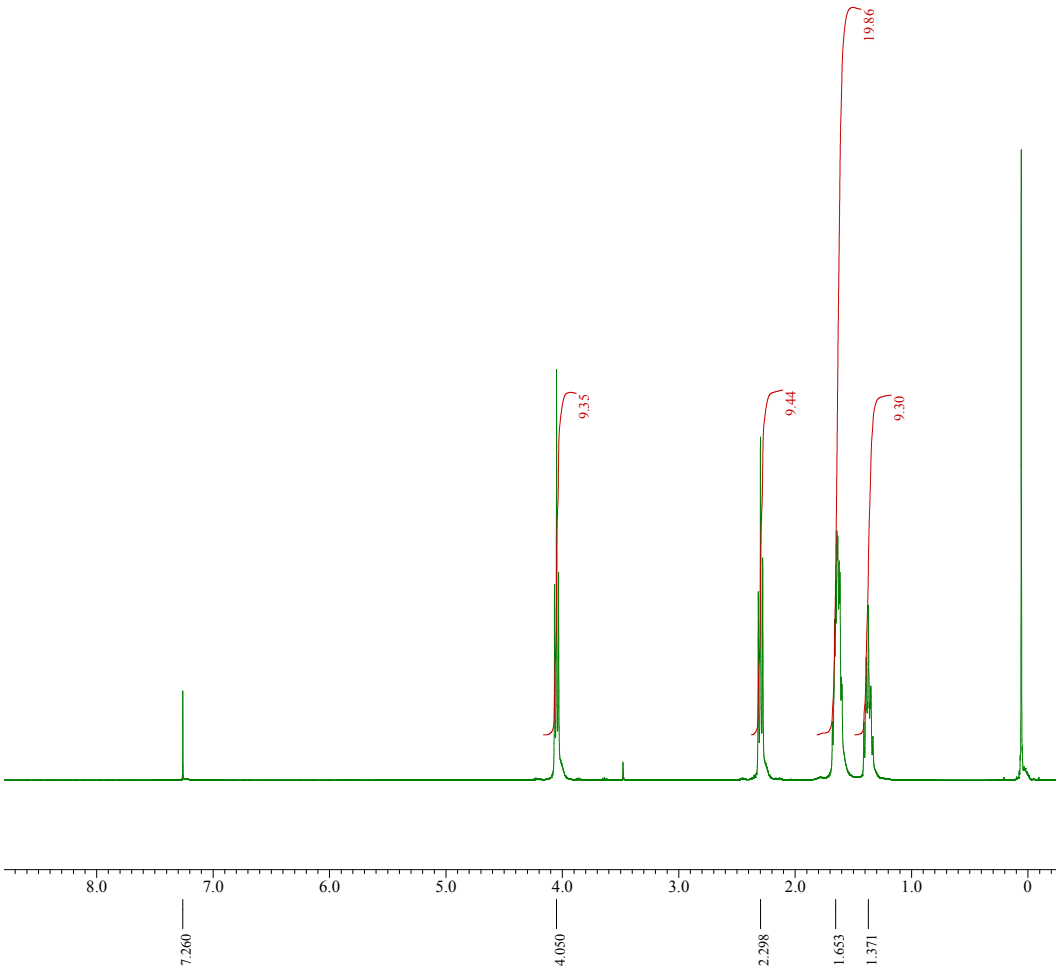

Figure S7 ^{1}H NMR spectrum ($CDCl_3$, 400 MHz, 298 K) of the PCL synthesised with **5** in the absence of BnOH under N_2.

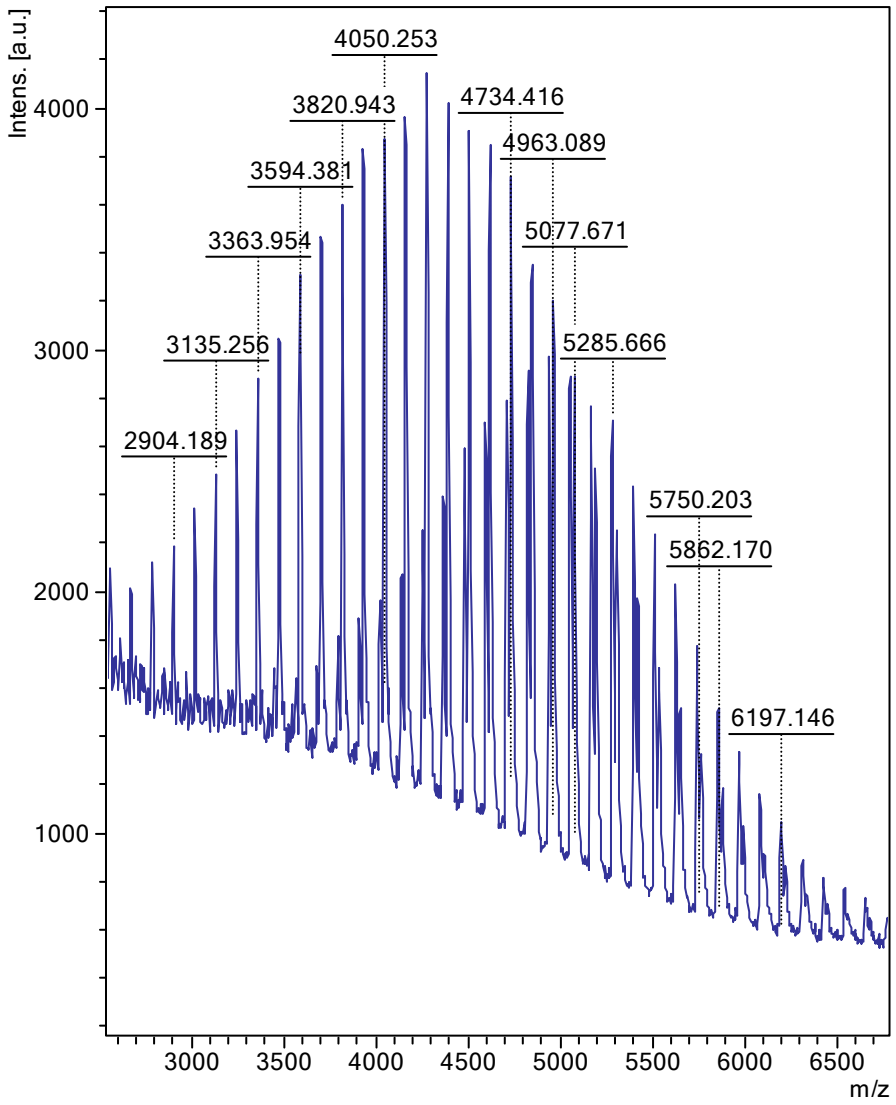

Figure S8. MALDI-TOF spectrum of the PCL synthesized with **5**/BnOH under N_2.

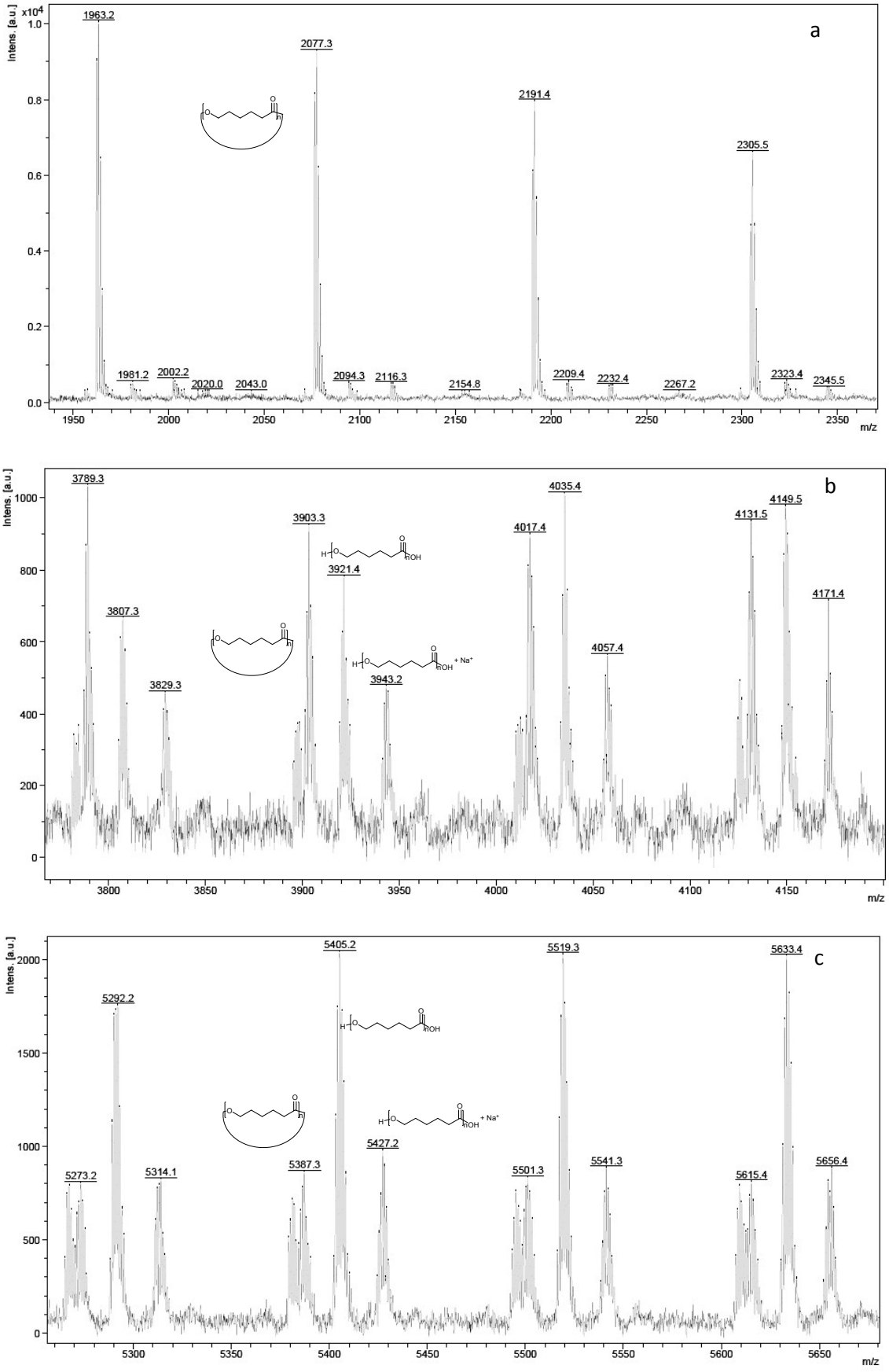

Figure S9. MALDI-TOF spectrum of the PCL synthesized with **5**/BnOH in air.

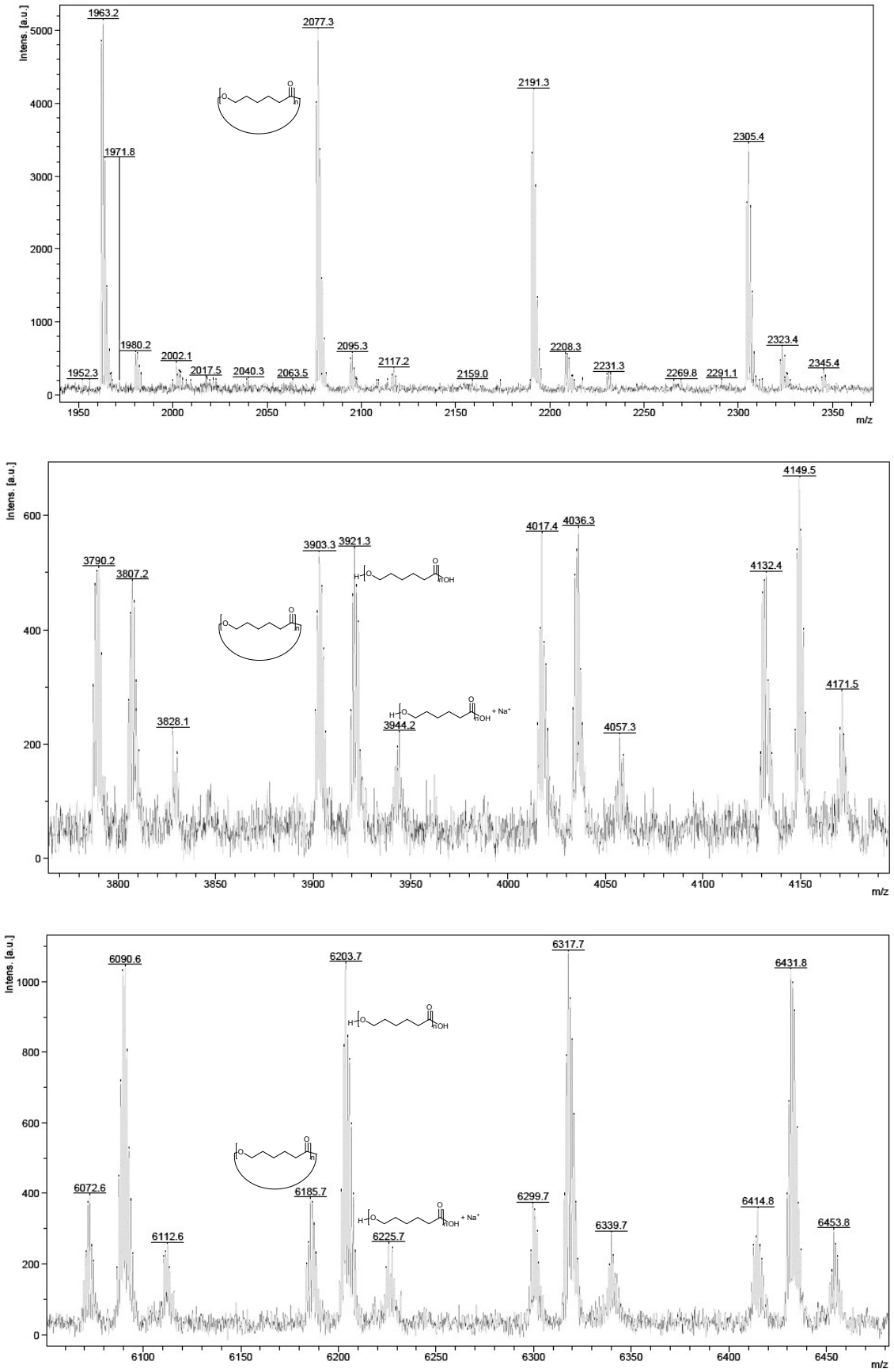

Figure S10. MALDI-TOF spectrum of the PCL synthesized with **5**/BnOH in the absence of BnOH under N_2.

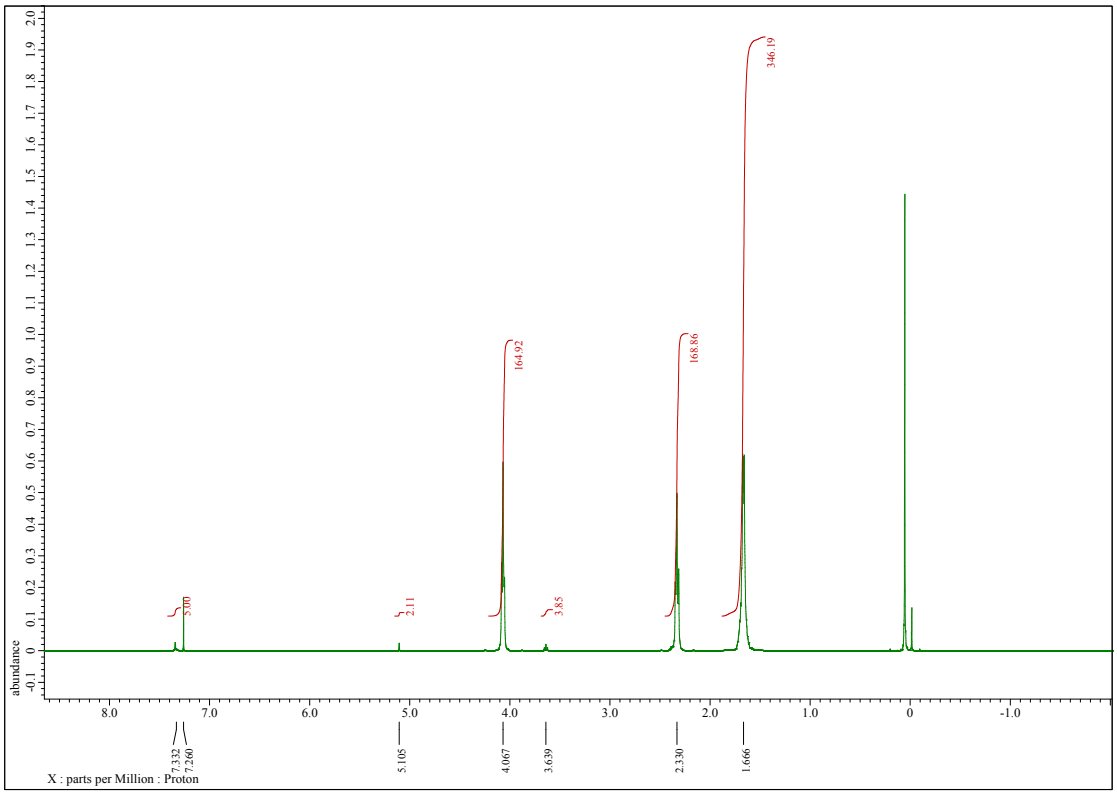

Figure S11: ^{1}H NMR spectrum ($CDCl_3$, 400 MHz, 298 K) of the PVL synthesised with **5**/BnOH uneder N_2.

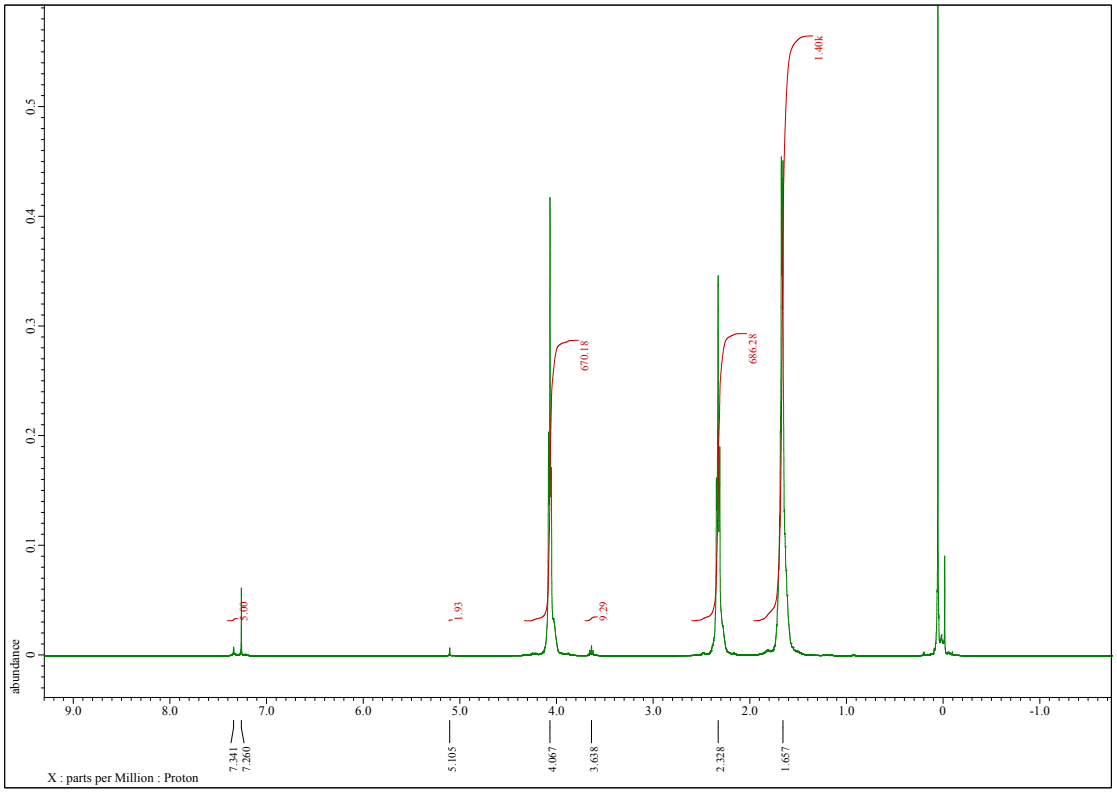

Figure S12: ^{1}H NMR spectrum ($CDCl_3$, 400 MHz, 298 K) of the PVL synthesized with **5**/BnOH in air.

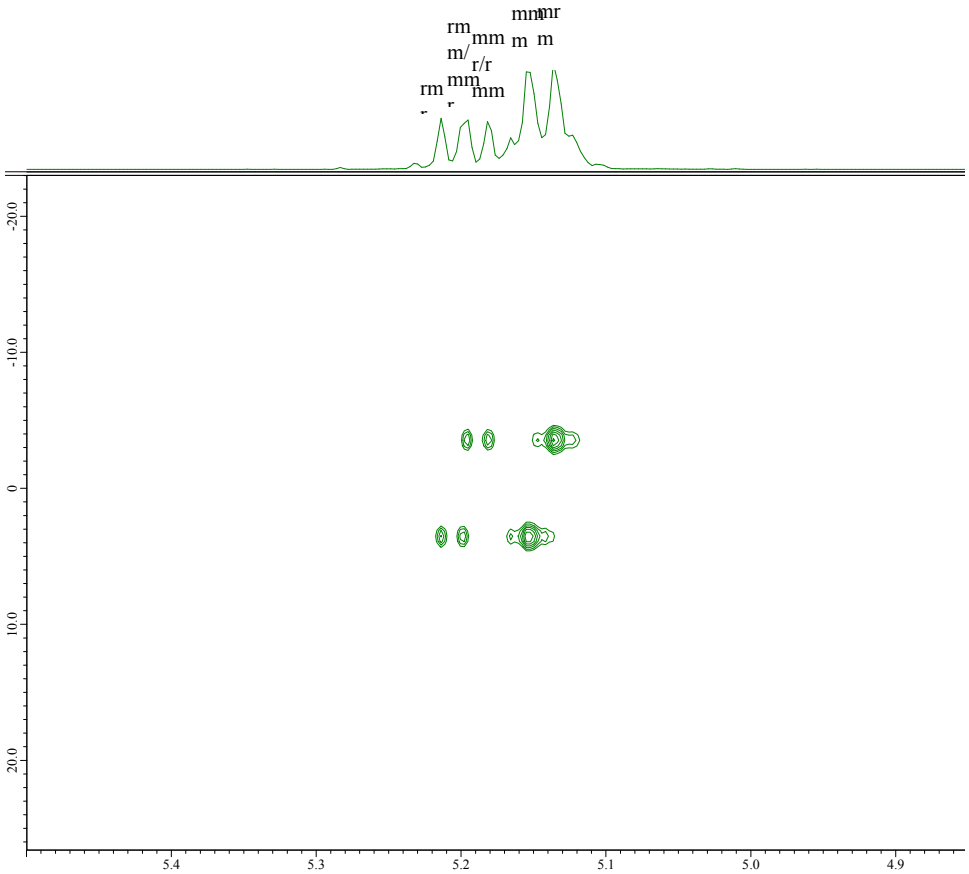

Figure S13: 2D J-resolved ^{1}H NMR spectrum ($CDCl_3$, 400 MHz, 298 K) of the PLA synthesized with **1**.

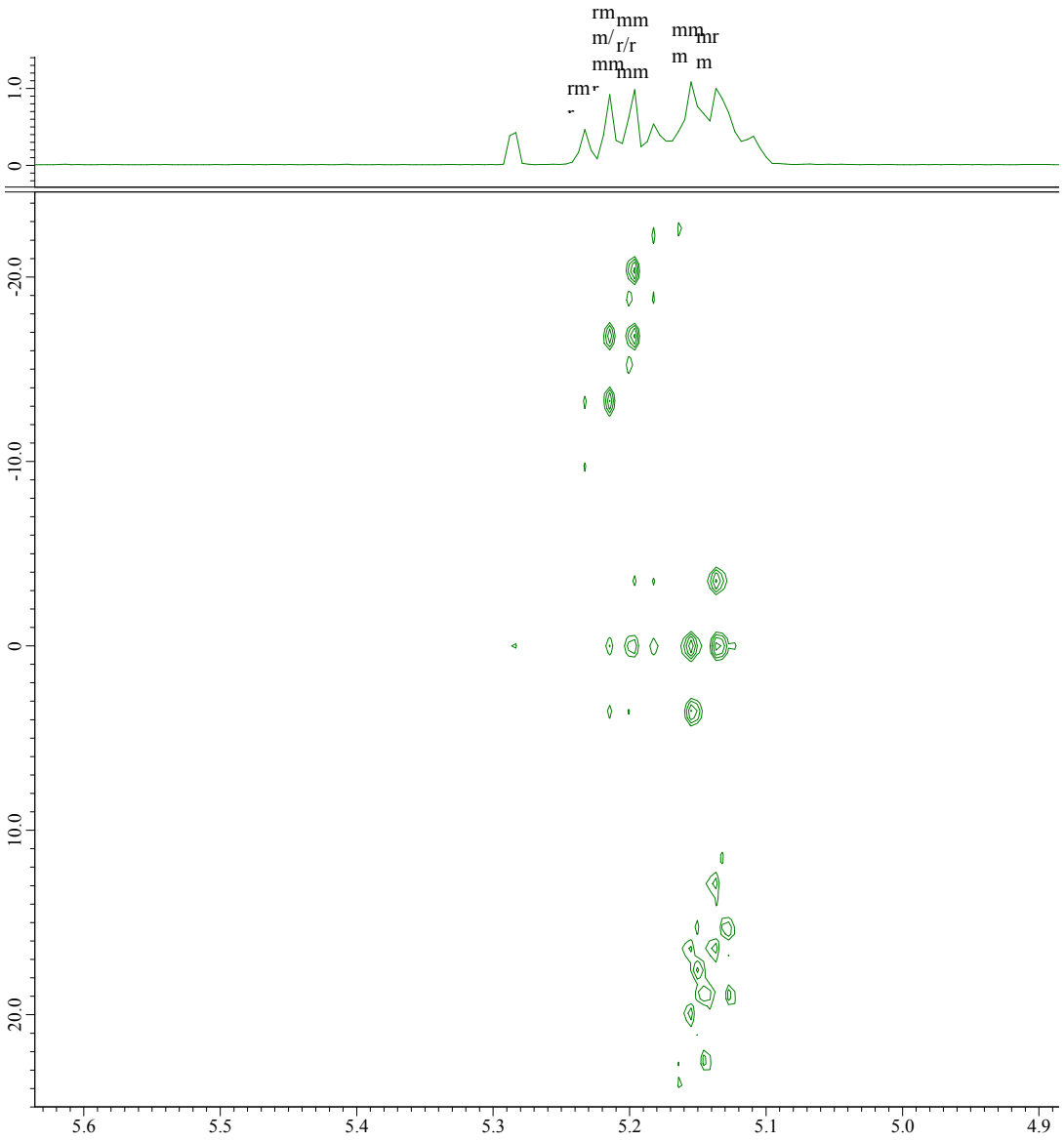

Figure S14: 2D J-resolved ^{1}H NMR spectrum ($CDCl_3$, 400 MHz, 298 K) of the PLA synthesized with **2**.

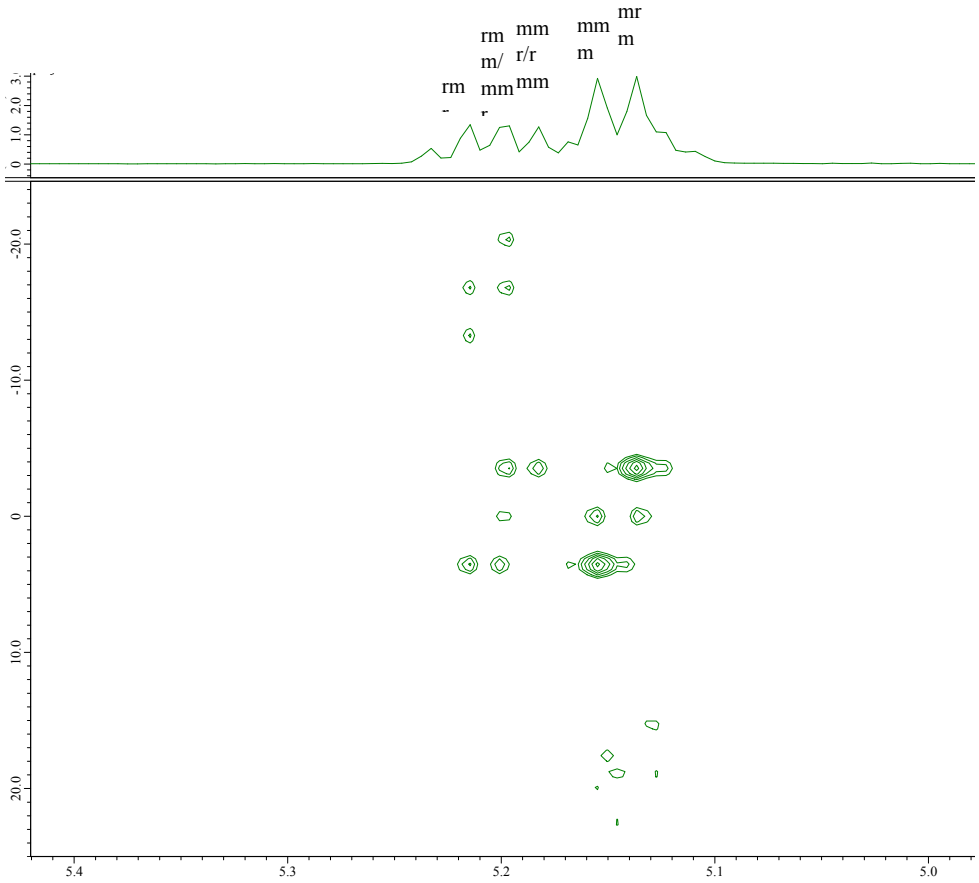

Figure S15: 2D J-resolved ^{1}H NMR spectrum ($CDCl_3$, 400 MHz, 298 K) of the PLA synthesized with **3**.

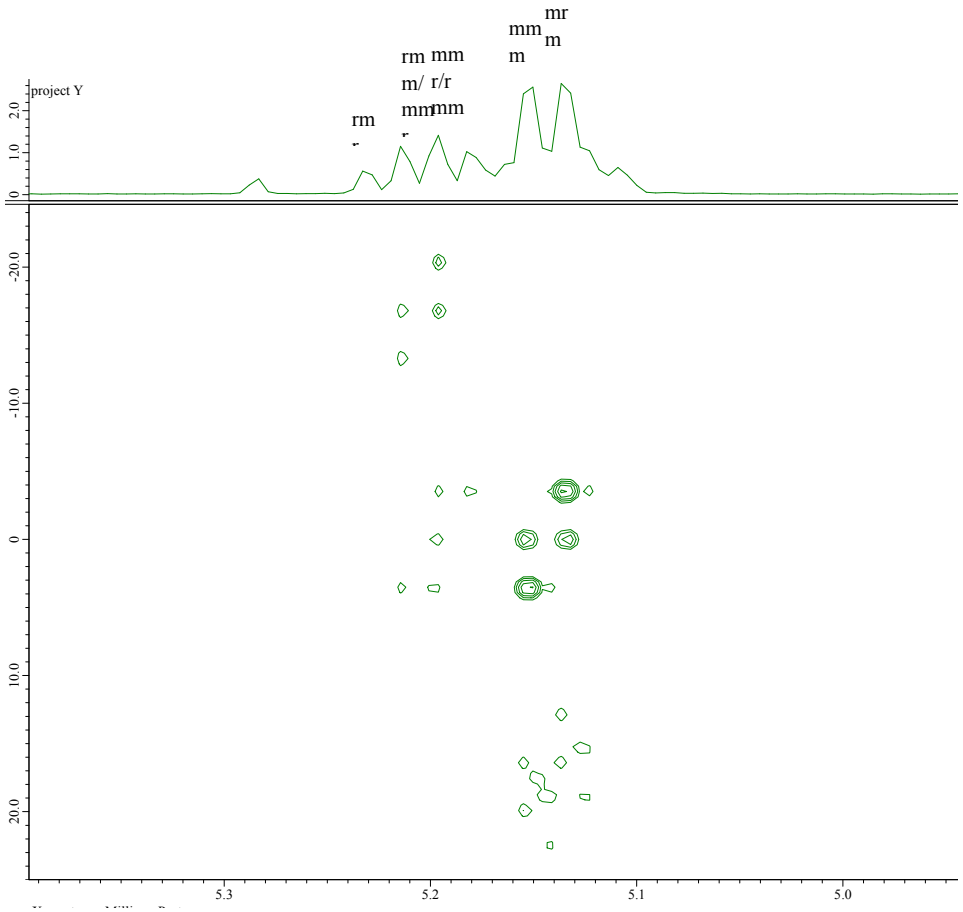

Figure S16: 2D J-resolved ^{1}H NMR spectrum ($CDCl_3$, 400 MHz, 298 K) of the PLA synthesized with **4**.

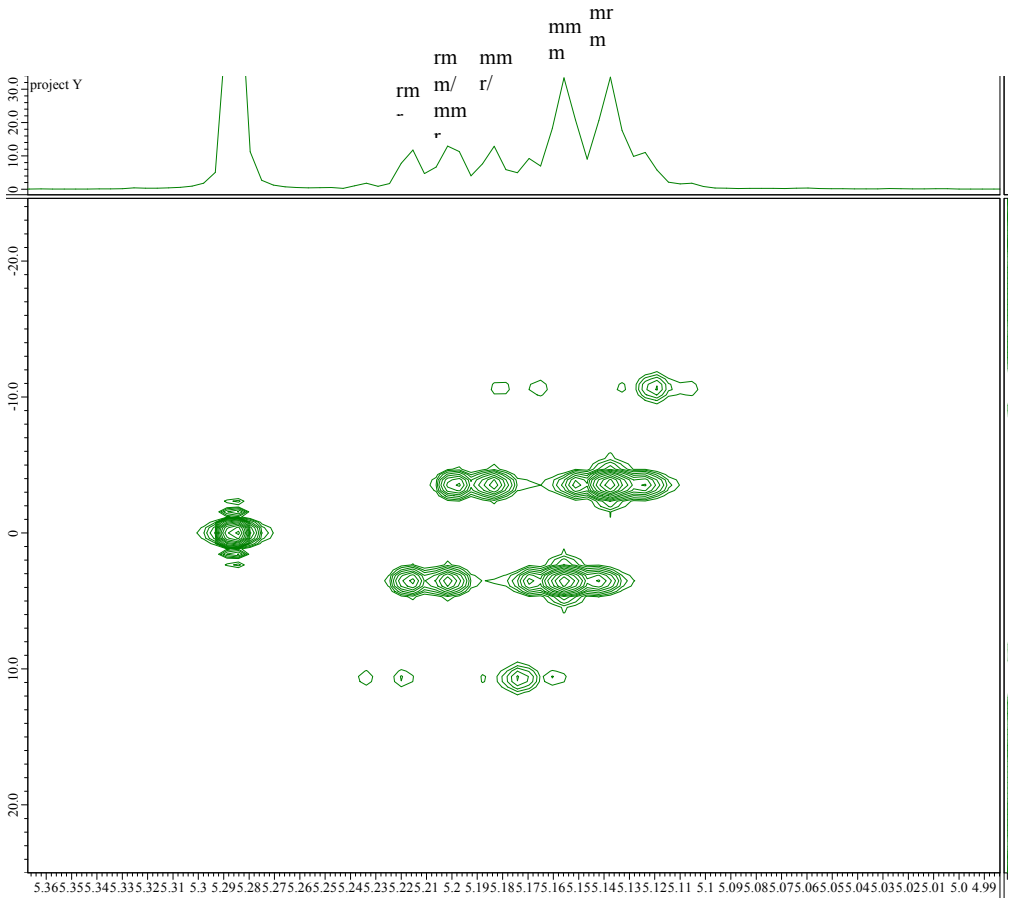

Figure S17: 2D J-resolved ^{1}H NMR spectrum ($CDCl_3$, 400 MHz, 298 K) of the PLA synthesized with **5**.

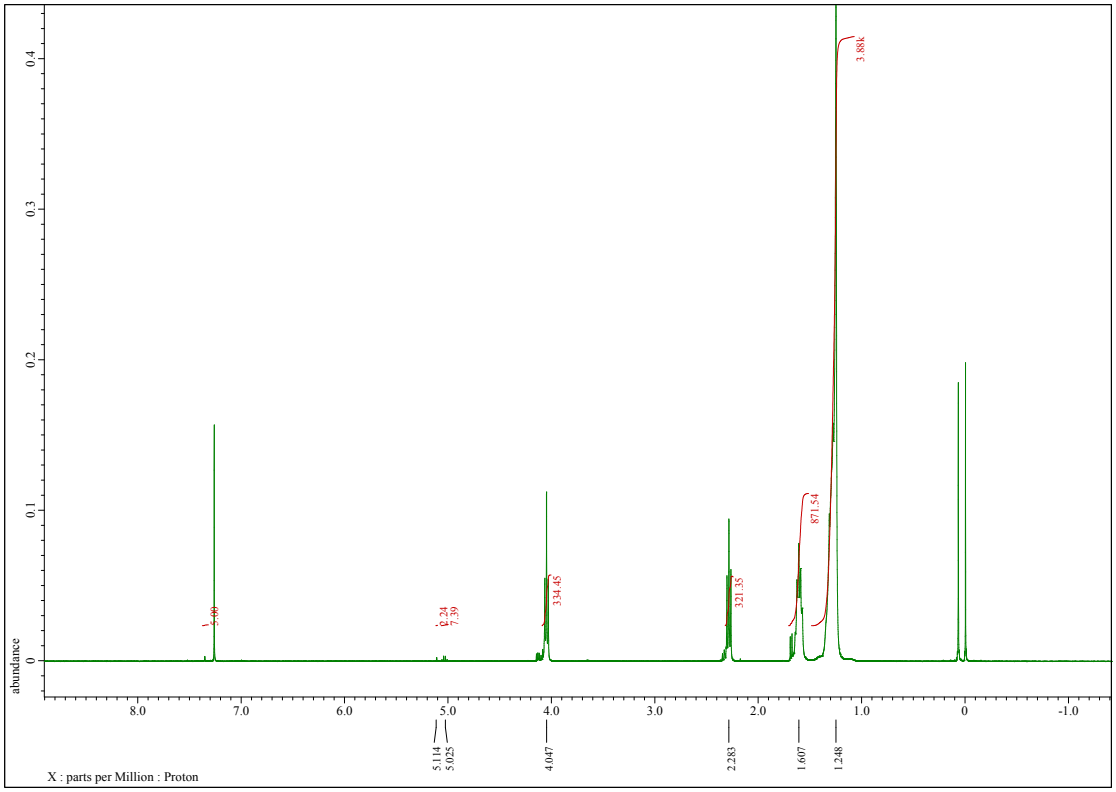

Figure S18: ^{1}H NMR spectrum ($CDCl_3$, 400 MHz, 298 K) of the poly-PDL.

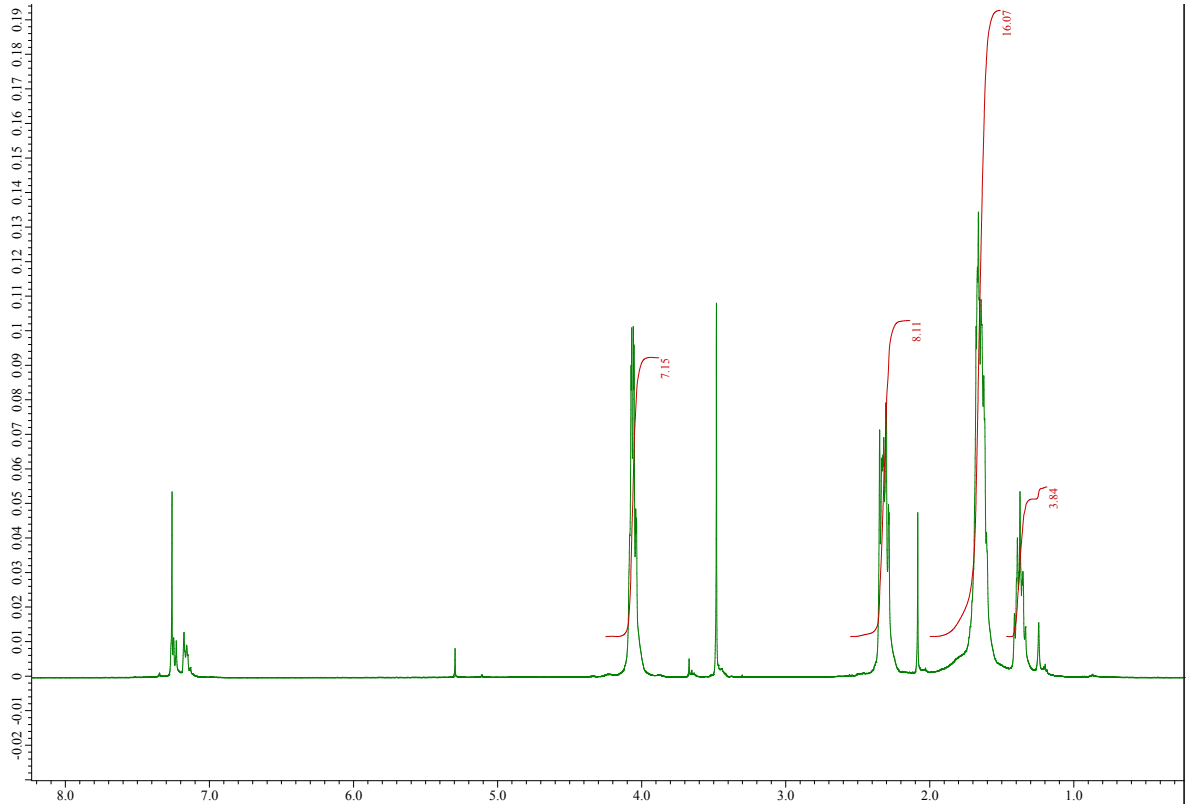

Figure S19: ^{1}H NMR spectrum ($CDCl_3$, 400 MHz, 298 K) of the CL-VL Copolymer (1:1 ratio CL/VL).

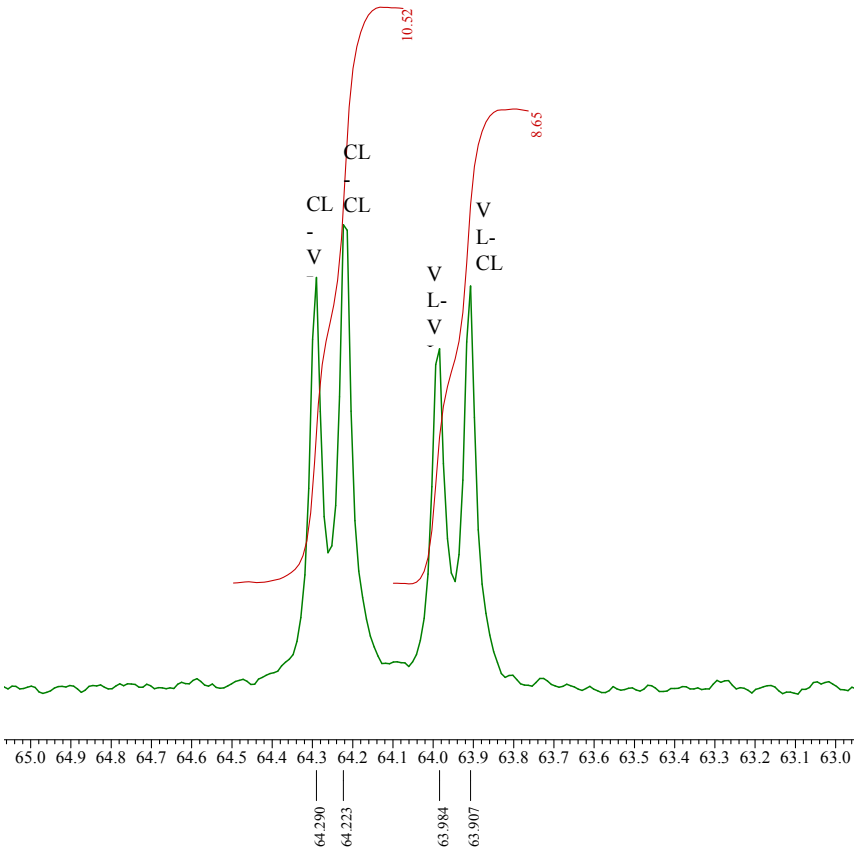

Figure S20. ^{13}C NMR spectrum (CDCl3, 400 MHz, 298 K) of the CL-VL Copolymer (65-63 ppm)

Equation S1 Determination of number-average sequence length for CL. [1]

$$L\mathrm{CL} = \frac{(I\mathrm{CL}\text{ - }\mathrm{CL})}{(I\mathrm{VL}\text{ - }\mathrm{CL})} + 1$$

Where $I_{CL\text{-}CL}$ and $I_{VL\text{-}CL}$ is the area of the peak belonging to the CL-CL and VL-VL dyad, respectively.

Equation S2. Determination of number-average sequence length for VL. [1]

$$L\mathrm{VL} = \frac{(I\mathrm{VL}\text{ - }\mathrm{VL})}{(I\mathrm{CL}\text{ - }\mathrm{VL})} + 1$$

Where $I_{VL\text{-}VL}$ and $I_{CL\text{-}VL}$ is the area of the peak belonging to the VL-VL and CL-VL dyad, respectively.

Equation S3. Determination of the Randomness Character (R). [1]

$$R = \frac{1}{L\mathrm{CL}} + \frac{1}{L\mathrm{VL}}$$

Completely block Copolymers: R = 0
Copolymers with a “blocking” tendency: R < 1
Completely random copolymers: R = 1
Copolymers with an alternating tendency: R >1
Completely alternating copolymers: R = 2

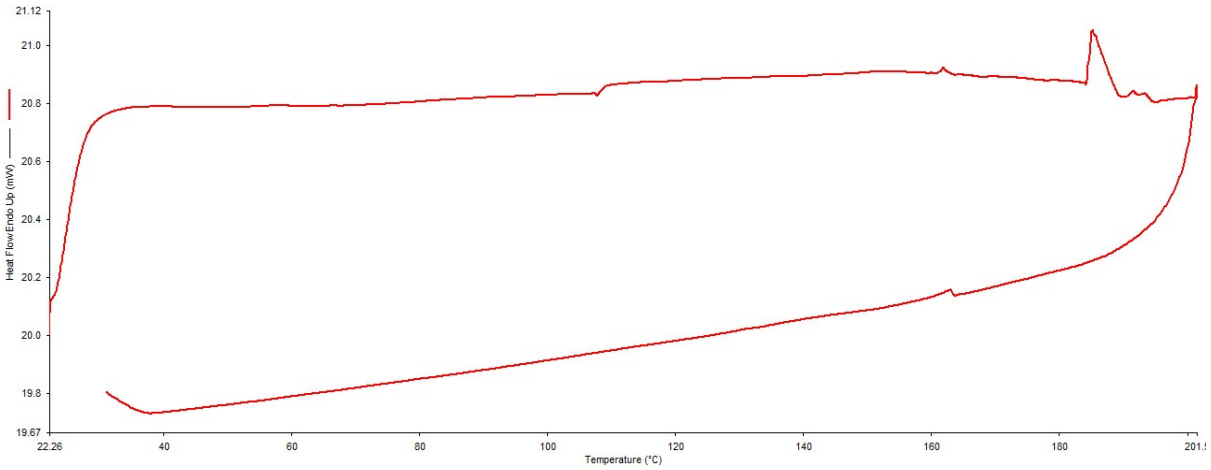

Figure S21. DSC curve of the CL/VL copolymer. Temperature range 23-190 ºC; Ramp 10ºC/min.

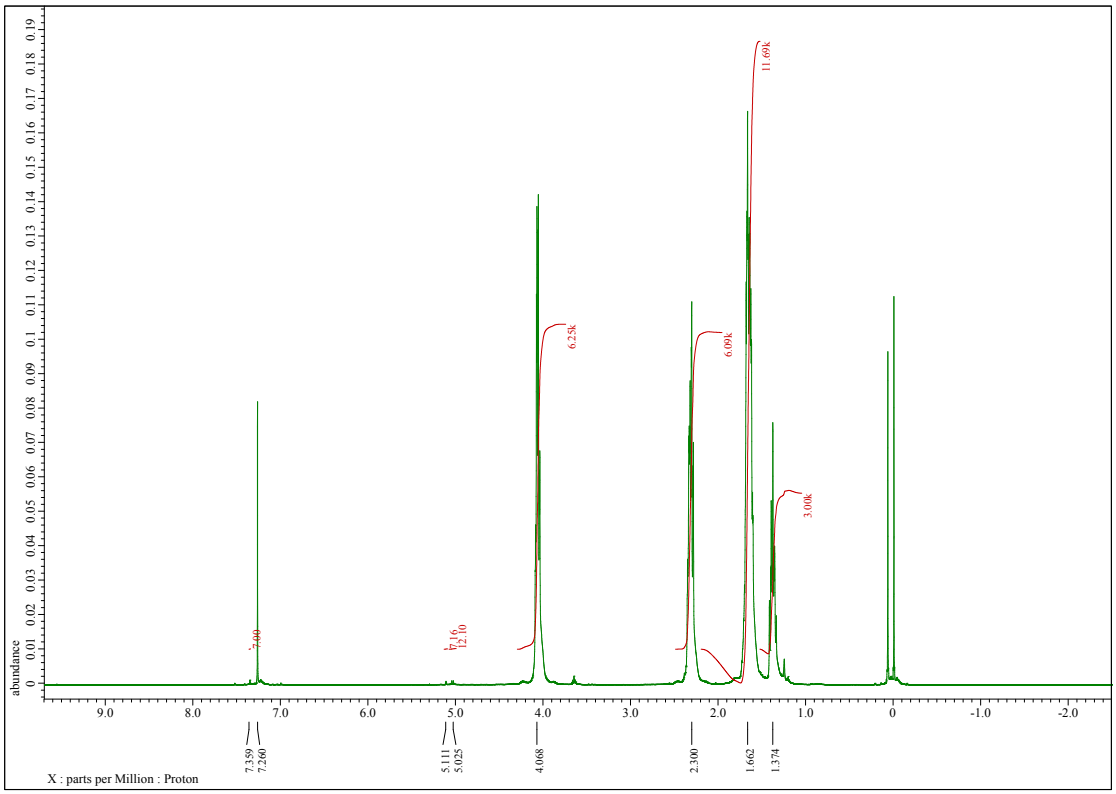

Figure S22. ^{1}H NMR spectrum ($CDCl_3$, 400 MHz, 298 K) of the CL/LA (500:50) co-polymer (mainly PCL).

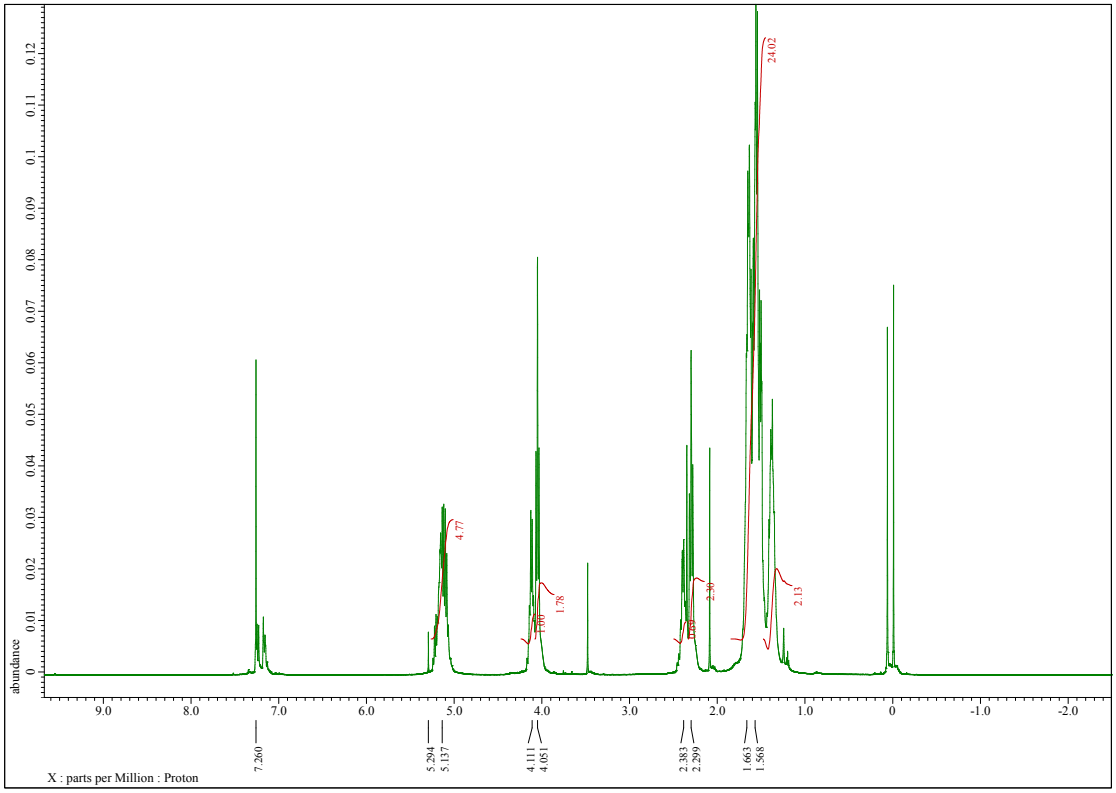

Figure S23. ^{1}H NMR spectrum ($CDCl_3$, 400 MHz, 298 K) of CL/LA co-polymer 75% PLA: 35% PCL – unreacted ε-CL).

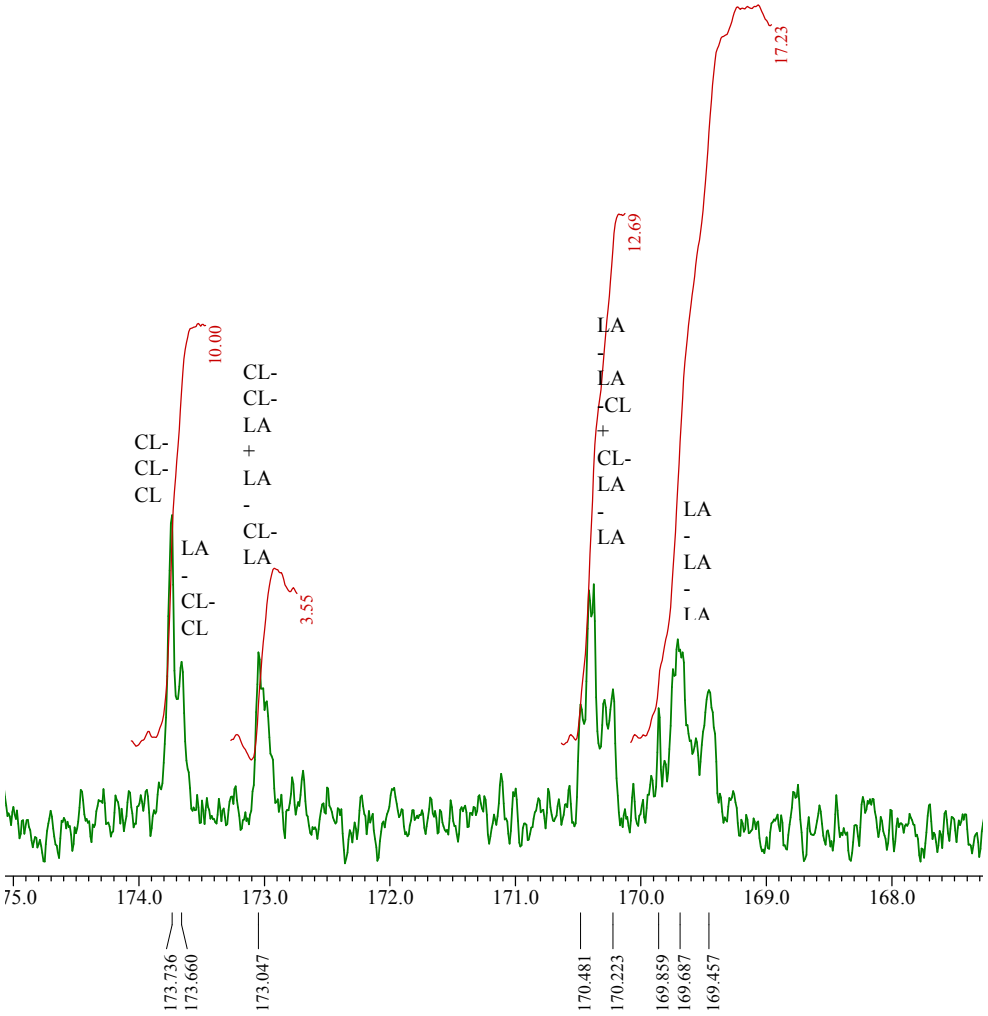

Figure S24. Carbonyl range of ^{13}C NMR spectrum ($CDCl_3$, 25 ºC) of CL/LA co-polymer 75% PLA: 35%. Triads have been assigned according to the literature. [2]

Equation S4. Determination of number-average sequence length for CL [2]

$$LCL = \left[\frac{(I\text{CLCLCL} + \text{LACLCL})}{(I\text{CLCLLA} + \text{LACLLA}} + 1\right]$$

Equation S5. Determination of number-average sequence length for LA [2]

$$LLA = \left[\frac{I\text{LALALA} + \left(\frac{I\text{LALACL} + \text{CLLALA}}{2}\right)}{\left(\frac{I\text{LALACL} + \text{CLLALA}}{2}\right) + I\text{CLLACL}} + 1\right] * \frac{1}{2}$$

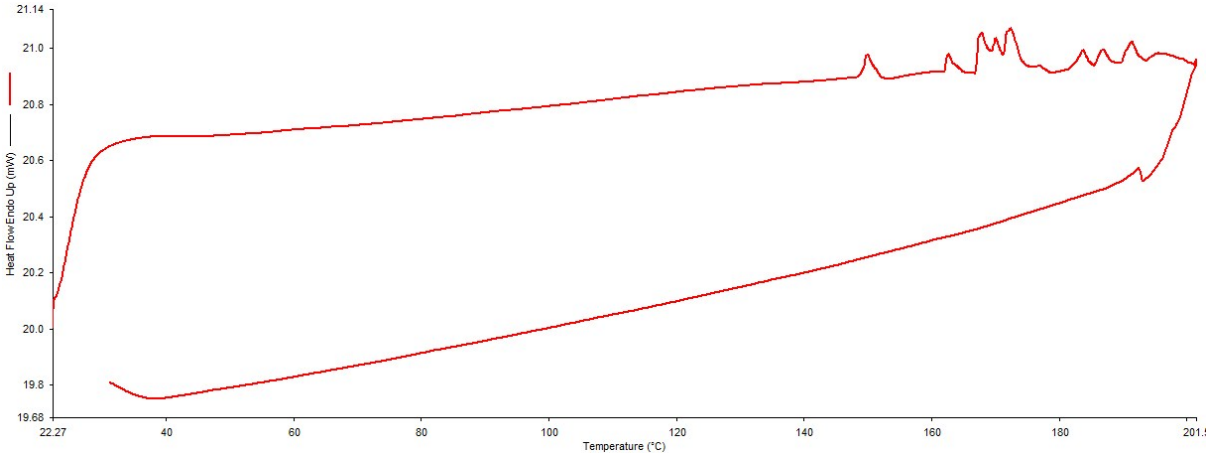

Figure S25. DSC curve of the CL/LA copolymer. Temperature range 23-190 ºC; Ramp 10ºC/min.

References

[1] (a) Q. Hu , S.-Y. Jie, P. Braunstein and B.-G. Lia *Chinese J. Polym. Sci*. **2020**, *38*, 240–247; (b) M. A. Woodruff and D. W. Hutmacher *Prog. Polym. Sci.* **2010**, *35*, 1217−1256; (c) T. Wu, Z. Wei, Y. Ren, Y. Yu, X. Leng and Y. Li *Polym. Degrad. Stab*. **2018**, 155, 173−182; (d) M. T. Hunley, N. Sari, and K. L. Beers, *ACS Macro Lett.* **2013**, *2*, 375−379.

[2] (a) F. Della Monica, E. Luciano, A. Buonerba, A. Grassi, S. Milione and Carmine Capacchione *RSC Adv.* **2014**, *4*, 51262−51267; (b) P. Vanhoorne, P. Dubois, R. Jerome and P. Teyssie *Macromolecules* **1992**, *25*, 37–44; (c) J. Kasperczyk and M. Bero, *Makromol. Chem*. **1991**, *192*, 1777–1787; (d) J. Kasperczyk and M. Bero, *Makromol. Chem*. **1993**, *194*, 913–925; (e) N. Nomura, A. Akita, R. Ishii and M. Mizuno *J. Am. Chem. Soc.* **2010**, *132*, 1750–1751; (f) G. Li, M. Lamberti, D. Pappalardo and Claudio Pellecchia *Macromolecules* **2012**, *45*, 8614−8620.